This article was downloaded by: [University of Haifa Library]
On: 11 August 2012, At: 10:53
Publisher: Taylor & Francis
Informa Ltd Registered in England and Wales Registered Number: 1072954
Registered office: Mortimer House, 37-41 Mortimer Street, London W1T 3JH, UK

Molecular Crystals and Liquid Crystals

Publication details, including instructions for authors and subscription information:
http://www.tandfonline.com/loi/gmcl20

Crystal Structures and Physical Properties of Cation Radical Salts of Ethylenedioxy-Ethylenedithio-Tetrathiafulvalene (Edoedt-Ttf Or Eoet): A ″-(Eoet) 2 Aubr 2 And β ″″-(Eoet) 2 Aubr 2

Yukihiro Yoshida [a], Takashi Aoki [a], Hiroshi Sasaki [a], Mineyuki Shiinoki [a], Hideki Yamochi [a] & Gunzi Saito [a]

[a] Division of Chemistry, Graduate School of Science, Kyoto University, Sakyo-ku, Kyoto, 606-8502, Japan

Version of record first published: 18 Oct 2010

To cite this article: Yukihiro Yoshida, Takashi Aoki, Hiroshi Sasaki, Mineyuki Shiinoki, Hideki Yamochi & Gunzi Saito (2003): Crystal Structures and Physical Properties of Cation Radical Salts of Ethylenedioxy-Ethylenedithio-Tetrathiafulvalene (Edoedt-Ttf Or Eoet): A ″-(Eoet) 2 Aubr 2 And β ″″-(Eoet) 2 Aubr 2, Molecular Crystals and Liquid Crystals, 393:1, 105-118

To link to this article: http://dx.doi.org/10.1080/15421400390202944

PLEASE SCROLL DOWN FOR ARTICLE

Full terms and conditions of use: http://www.tandfonline.com/page/terms-and-conditions

This article may be used for research, teaching, and private study purposes. Any substantial or systematic reproduction, redistribution, reselling, loan, sub-licensing, systematic supply, or distribution in any form to anyone is expressly forbidden.

The publisher does not give any warranty express or implied or make any representation that the contents will be complete or accurate or up to date. The accuracy of any instructions, formulae, and drug doses should be independently verified with primary sources. The publisher shall not be liable for any loss, actions, claims, proceedings, demand, or costs or damages whatsoever or howsoever caused arising directly or indirectly in connection with or arising out of the use of this material.

Downloaded by [University of Haifa Library] at 10:53 11 August 2012

Mol. Cryst. Liq. Cryst., Vol. 393, pp. 105–118
Copyright © 2003 Taylor & Francis
1542-1406/03 $12.00 + .00
DOI: 10.1080/15421400390202944

Taylor & Francis
Taylor & Francis Group

CRYSTAL STRUCTURES AND PHYSICAL PROPERTIES OF CATION RADICAL SALTS OF ETHYLENEDIOXY-ETHYLENEDITHIO-TETRATHIAFULVALENE (EDOEDT-TTF OR EOET): α'-$(EOET)_2AuBr_2$ AND β''-$(EOET)_2AuBr_2$

Yukihiro Yoshida, Takashi Aoki, Hiroshi Sasaki, Mineyuki Shiinoki, Hideki Yamochi, and Gunzi Saito
Division of Chemistry, Graduate School of Science, Kyoto University, Sakyo-ku, Kyoto 606-8502, Japan

The crystal and calculated band structures and electric, magnetic, and optical properties of two cation radical salts of ethylenedioxy-ethylenedithio-tetrathiafulvalene (EDOEDT-TTF: EOET): α'-$(EOET)_2AuBr_2$ and β''-$(EOET)_2AuBr_2$, are described. The α' salt is a Mott insulator with an EOET dimer as a unit with an $S = 1/2$ spin. The dimers form a two-dimensional square lattice layer. The spin dynamics follow the quadratic layer antiferromagnetic model above 60 K and then pass through a three-dimensional antiferromagnetic transition at around 9 K. The β'' salt shows a metallic behavior down to low temperatures.

Keywords: ethylenedioxy-ethylenedithio-TTF (EOET); cation radical salt; crystal structure; conductivity; self-assembling ability; Mott insulator; antiferromagnetic ordering

Downloaded by [University of Haifa Library] at 10:53 11 August 2012

INTRODUCTION

The bis(ethylenedithio)-tetrathiafulvalene (BEDT-TTF or ET, Figure 1) molecule and its ethylenedioxo analogue (bis(ethylenedioxy)-TTF, BEDO-TTF or BO) have afforded a number of two-dimensional (2D) conductive materials [1]. With inorganic anions, ET has produced more than 50 superconductors while BO has produced only two. With organic acceptor molecules, BO has provided a large number of 2D metals even in severely disordered systems [2, 3], while ET has given not so many metallic

This work was supported in part by a COE Research on Elements Science from the Ministry of Education, Culture, Sports, Science and Technology, Japan (No. 12CE2005) and a fund from NEDO. E-mail: yoshiday@kuchem.kyoto-u.ac.jp or Saito@kuchem.kyoto-u.ac.jp

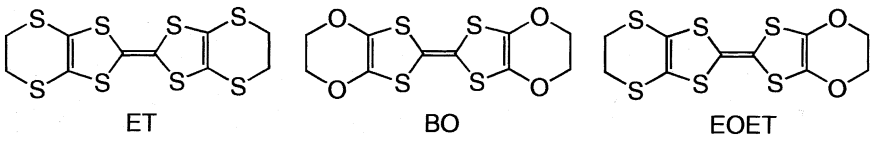

FIGURE 1 Chemical structures of the ET, BO, and EOET molecules.

compounds which are unstable against disorder. These facts indicate that the electronic and structural features of the 2D BO-based metals are stable against phase transitions, including metal-insulator and metal-superconductor transitions, in comparison to those of the 2D ET-based metals.

The metallic character of the BO compounds originates from the intermolecular interactions based on both the CH··O hydrogen bonds along the stacking axis and the S_{in}··S_{in} atomic contacts oblique to the stacking axis, providing a structurally and electronically stable 2D assembly of limited numbers of donor packing patterns (self-assembling ability), where S_{in} is the sulfur atoms in the TTF moiety [2]. On the other hand, the 2D nature of the ET compounds is ascribed to the compromise between the side-by-side and face-to-face intermolecular interactions in the ET layer. Along with the donor··donor interactions, the donor··anion and anion··anion interactions play essential roles in complex formation, resulting in the multiple phases of ET compounds [1].

The hybrid molecule of the ET and BO molecules, ethylenedioxyethylenedithio-TTF (EDOEDT-TTF or EOET), is characterized by a lower molecular symmetry (C_{2v}) than both parent molecules (D_{2h}) and a reduced self-assembling ability with respect to the BO molecules. In the previous report we have demonstrated that the EOET compounds with organic acceptor molecules have diversity in their electronic and structural aspects [4].

The high solubility of EOET in conventional organic solvents has prevented solid cation radical salts from being obtained by electrocrystallization. So far, the specified studies on the structural and physical properties of EOET salts have been reported [5–10], namely the structural ones of AuI_2 salts (τ-($\sim$1:1), α-(2:1)) [5] and Hg_3Br_8 [6], conductivity results of AuI_2(τ-, α-phases) [5], $Cu(NCS)_2$ (2:1) [5, 7], $Pt(CN)_4$ (4:1) [8] and $Pd(CN)_4$ [8] salts, and preparation of I_3 and IBr_2 salts [9]. We report here the structural and physical properties of the cation radical salts of EOET with $AuBr_2$: α'- and β''-phases. Brief reports were made previously [10].

EXPERIMENTAL

Black needles (α'-phase, $2 \times 0.05 \times 0.05\,mm^3$) and blocks (minor product, β''-phase, $0.5 \times 0.5 \times 0.5\,mm^3$) were harvested simultaneously by the

Downloaded by [University of Haifa Library] at 10:53 11 August 2012

electrooxidation of EOET using tetrabutylammonium-AuBr$_2$ in 1,2-dichloroethane with a constant current (0.5 μA) in an 18 mL H-shaped cell at room temperature (RT) and then separated from each other under microscope. Their crystallographic data are summarized in Table I.

The optical measurements at RT were carried out on a Perkin-Elmer 1000 Series Fourier transform infrared (FTIR) for IR and near-IR (NIR) regions (400–7800 cm^{-1}) in KBr, and on a SHIMADZU UV-3100 spectrometer for UV-Vis-NIR region (3800–42000 cm^{-1}) in KBr or methanol. The d.c. conductivity was measured using a standard four- or two-probe technique attaching gold wires (15 μmϕ) on a crystal by gold paint (Tokuriki 8560-1A). The magnetic susceptibility measurements were performed using a SQUID (Quantum Design MPMS-XL) on the polycrystalline sample and using an EPR X-band spectrometer (JEOL-TE200) equipped with a TE_{011} cavity on a single crystal. In the latter case, the absolute value of the spin susceptibility (χ_{spin}) was determined with reference to the signal of $CuSO_4{\cdot}5H_2O$. The X-ray diffraction data were collected on an automatic four-circle diffractometer (MacScience, MXC^Z) or an oscillator-type X-ray imaging plate (MacScience DIP 2020K) with monochromated MoKα radiation at RT. The refinements of the structures were performed by full matrix least squares method (SHELXL-97). The position of hydrogen

TABLE I Crystallographic Data for (EOET)$_2$X Salts

Salt	α′-(EOET)$_2$AuBr$_2$	β″-(EOET)$_2$AuBr$_2$
Formula	$C_{20}H_{16}AuBr_2O_4S_{12}$	$C_{20}H_{16}AuBr_2O_4S_{12}$
Crystal shape	black needle	black block
Crystal system	triclinic	triclinic
Space group	$P\bar{1}$	$P\bar{1}$
a [Å]	6.580(3)	5.245(1)
b [Å]	7.267(3)	8.983(2)
c [Å]	16.641(5)	16.127(4)
α [°]	77.31(3)	92.36(1)
β [°]	88.93(2)	97.92(1)
γ [°]	84.98(3)	104.61(1)
V [Å^3]	773.3(5)	746.5(3)
Z	1	1
ρ_{calc} [g cm^{-3}]	2.28	2.36
T [K]	298	298
$2\theta_{max}$ [°]	55	55
Criterion for obs. reflection	$F_0 \geq 4\sigma\ (F_0)$	$F_0 \geq 4\sigma(F_0)$
Reflections used	1776	2287
Parameters refined	198	178
R	0.056	0.054

CIF files for α′-(EOET)$_2$AuBr$_2$ (#196949) and β″-(EOET)$_2$AuBr$_2$ (#196950) have been deposited with the Cambridge Crystallographic Data Center.

Downloaded by [University of Haifa Library] at 10:53 11 August 2012

atoms was determined assuming an sp^3 configuration with a C-H distance of 1.0 Å. The band structures were calculated based on an extended Hückel method with the tight binding approximation using single-ζ parameters excluding 3d orbitals of sulfur atoms [11].

RESULTS AND DISCUSSION

α'-$(EOET)_2AuBr_2$

Two half EOET molecules and half of the anion molecule are crystallographically independent. Namely, the sulfur and oxygen atoms in the outer six-member ring (X_{out}) of EOET molecules cannot be distinguished from each other. Also, the terminal ethylene groups are conformationally disordered. The EOET molecules form a twisted stack, α'-phase in the ET system [12], along the *b*-axis with interplanar spacing of 3.62 Å, as shown in Figure 2a. Along the side-by-side direction, there are short heteroatomic contacts less than the sum of the van der Waals radii [13] for $S_{in}\cdot\cdot X_{out}$ and $X_{out}\cdot\cdot X_{out}$ but not for $S_{in}\cdot\cdot S_{in}$ (Figure 2b). Since the electron density on the X_{out} atoms is much less than on the S_{in} ones, the transverse transfer interactions in this salt are not so effective. These structural data are indicative of the reduced self-assembling nature of EOET compared to that of BO.

The UV-Vis-NIR spectrum of the salt in KBr (Figure 3, curve a) exhibits absorption bands at $3.5\times10^3\,cm^{-1}$ (labeled A) and at $11.0\times10^3\,cm^{-1}$ (labeled C), and shoulders at around 17×10^3 (labeled D), 20×10^3 and $30–33\times10^3\,cm^{-1}$. The bands above $10\times10^3\,cm^{-1}$ are readily assigned to the intramolecular transitions of EOET cation radical molecules when compared with the absorption bands observed for $(EOET)_5Br_3(H_2O)_6$ in methanol (curve c); 10.8×10^3 (2nd HOMO-HOMO, C), 16.7×10^3 (HOMO-LUMO, D), and $20.5–21.5\times10^3$, 30.6×10^3, and $32.1\times10^3\,cm^{-1}$. The band A is ascribed to the transition between partially charged EOET molecules

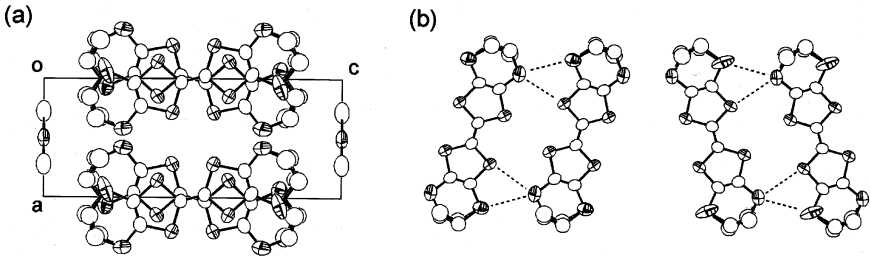

FIGURE 2 (a) Crystal structure and (b) side-by-side atomic contacts shorter than the sum of the van der Waals radii (shown by dotted lines) of α'-$(EOET)_2AuBr_2$.

Downloaded by [University of Haifa Library] at 10:53 11 August 2012

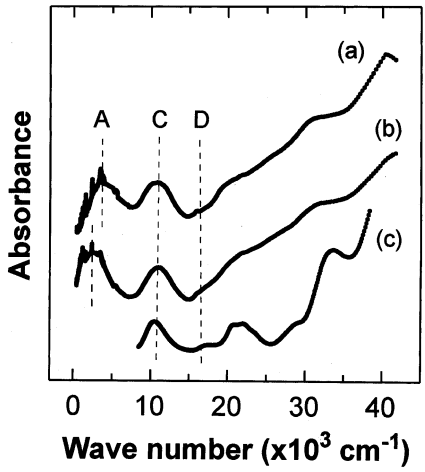

FIGURE 3 UV-Vis-NIR optical absorption spectra of (a) α′-(EOET)$_2$AuBr$_2$ and (b) β″-(EOET)$_2$AuBr$_2$ in KBr are compared with that of (c) (EOET)$_5$Br$_3$(H$_2$O)$_6$ in methanol.

in accordance with the 2:1 stoichiometry which affords a formally 3/4 filled valence band.

The salt is semiconductive with a RT conductivity of $\sigma_{RT} = 4.7 \times 10^{-3}$ S cm^{-1} and an activation energy of $\varepsilon_a = 220$ meV in spite of the almost uniform column of spin-1/2 EOET dimers along the segregated stack. The static susceptibility is 1.0×10^{-3} emu mol^{-1} at RT and increases down to 120 K followed by a gradual decrease down to 14 K as shown in Figure 4. At low temperatures, this salt shows a Curie-tail and thus it is difficult to determine the magnetic ground state. The temperature dependence is expressed by either the Bonner-Fisher model [14] with $|J|/k_B = 90$ K (dotted line) or the quadratic layer antiferromagnet (QLAF) model [15] with $|J|/k_B = 60$–70 K (solid line). These results indicate that the salt is not a band insulator but a Mott insulator similar to those of the α′-(ET)$_2$X (X = AuBr$_2$, Ag(CN)$_2$, CuCl$_2$, hydrogen cyananilate, etc) [12].

The origin of the semiconductive behavior of this salt is ascribed to the strong electron correlation with respect to the narrow bandwidth. The σ_{RT} value of 4.7×10^{-3} S cm^{-1} is comparable to those of Mott insulators α′-(ET)$_2$X (X = CuCl$_2$, Ag(CN)$_2$[12f], IAuBr[12b], *p*-CH$_3$C$_6$H$_4$SO$_3$[12c], HCl$_2$[12g] and alkoxytetracyanoallylide (alkyl: methyl, ethyl and butyl) [12h]; $\sigma_{RT} = 2 \times 10^{-4}$–$3 \times 10^{-3}$ S cm^{-1}), however it is less than those of Mott insulators α′-(ET)$_2$X (X = AuBr$_2$[12f], pentacyanodicyclopentadienide-(solvent)$_x$[12d] and hydrogen cyananilate[12i]; $\sigma_{RT} = 1$–5×10^{-1} S cm^{-1}). The ε_a value of 0.22 eV is similar to those of the above-mentioned Mott

Downloaded by [University of Haifa Library] at 10:53 11 August 2012

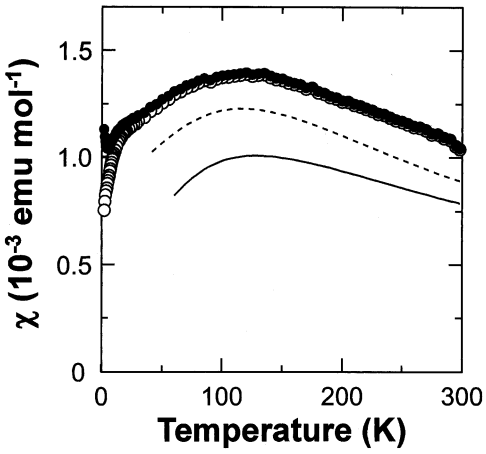

FIGURE 4 Temperature dependence of the static magnetic susceptibility at 3 kOe for α'-$(EOET)_2AuBr_2$ (closed circles). Open circles indicate data after the subtraction of the Curie impurities (0.2%). Dotted and solid lines represent the calculated susceptibilities for the Bonner-Fisher model with $|J|/k_B = 90\,K$ and the quadratic layer antiferromagnet model with $|J|/k_B = 70\,K$, respectively.

Downloaded by [University of Haifa Library] at 10:53 11 August 2012

insulators (0.10–0.30 eV), suggesting that α'-$(EOET)_2AuBr_2$ is one of the typical organic Mott insulators.

Taking these results into account, the spin dynamics of this system are discussed in relation to the spin geometry. For a 2:1 Mott insulator, the band structure based on the one-electron approximation should afford an energy split of the formally 3/4 filled HOMO band into upper and lower bands in order to realize an electron correlated 1/2 filled system [12]. Among the possible 16 patterns of donor orientations in a doubled unit cell, only the patterns depicted in Figure 5a, where open and shaded rectangles represent an EOET molecule projecting the ethylenedioxy group to opposite directions along the *c*-axis, afford a distinct energy split of the HOMO band as expected from the experimental results. It is thus likely that the main domain of the crystal consists of the EOET molecules arranged parallel within the column and antiparallel along the inter-stack direction.

In this case, the intra-dimer transfer integrals, t_{s2} and t_{s3}, are effectively larger than the inter-dimer ones, t_{s1}, t_{s4}, t_{p1-4}, and thus an EOET dimer with an $S = 1/2$ spin is the building unit of the spin system. Figure 5b shows a schematic view of the spin geometry where a circle represents a dimer unit. The ratio of the inter-dimer exchange interactions $(|t_{s1}|^2 + |t_{s4}|^2)/2 : (|t_{p1}|^2 + |t_{p4}|^2)/2 : (|t_{p2}|^2 + |t_{p3}|^2)/2 \approx 10{:}6{:}1$) indicates that the system can be described as a 2D square lattice layer rather than 1D chains. The ratio of $t'/t = 0.35$ (Figure 5b, t and t' are the averaged ones), where $t'/t = 1$ is the

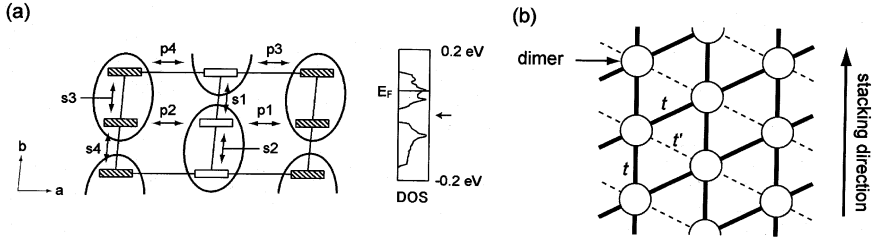

FIGURE 5 (a) Schematic donor orientation in two neighboring unit cells and corresponding density of states (DOS) for α′-(EOET)$_2$AuBr$_2$. Open and shaded rectangles represent EOET molecules with different orientations to each other and an ellipsoid represents a dimer unit with an $S = 1/2$ spin. A horizontal arrow beside DOS shows the energy split. Transfer integrals ($\times 10^{-2}$ eV) are: $t_{s1} = -3.4$, $t_{s2} = -7.2$, $t_{s3} = -7.2$, $t_{s4} = -3.4$, $t_{p1} = 2.7$, $t_{p2} = 0.8$, $t_{p3} = 1.3$, $t_{p4} = 2.4$. (b) Schematic square spin-geometry based on a spin-1/2 EOET dimer (circle). Solid and dotted lines linking the circles represent the transfer interactions with the absolute value more than 2×10^{-2} eV (t) and less than 2×10^{-2} eV (t'), respectively.

Downloaded by [University of Haifa Library] at 10:53 11 August 2012

triangular lattice and $t'/t = 0$ is the square lattice, is appreciably smaller than the value of 0.75 for a Mott insulator κ-(ET)$_2$Cu[N(CN)$_2$]Cl, which shows a weak ferromagnetic ordering caused by the spin canting below 27 K [16]. The observed Mott-insulating behavior is readily explained by the estimation of the W/U_{eff} value (W: bandwidth of upper HOMO band, U_{eff}: on-site Coulomb energy on an EOET dimer). The W value is estimated to be 0.11 eV. While the U_{eff} value is expressed as $U_{\mathrm{eff}} = 2|t_{\mathrm{dimer}}| + [U_0 - (U_0 + 16|t_{\mathrm{dimer}}|^2)^{1/2}]/2 \approx 2|t_{\mathrm{dimer}}|$, since $U_0 \gg |t_{\mathrm{dimer}}|$ for ET derivatives, where U_0 is the on-site Coulomb repulsion on an EOET molecule. The intra-dimer transfer energy $|t_{\mathrm{dimer}}|$, which corresponds to $(|t_{s2}| + |t_{s3}|)/2$ for α′-(EOET)$_2$ AuBr$_2$, is estimated to be 0.072 eV, leading to $W/U_{\mathrm{eff}} = 0.8$. This value is sufficiently smaller than unity, indicating the localized nature of the spins.

The α′ salt showed a single EPR signal with a Lorentzian-shape at $g \sim 2$ along all measured directions; the crystallographic a*-, b-, and c*-axes. Figure 6 shows the angular dependence of the g-factors at RT with the static magnetic field being applied within the a*b-, bc*-, and c*a*-planes. The solid curves are the least squares fit of the measured data using the standard anisotropic g-tensor equations, $g^2 = \sum_{i,j} G_{\mathrm{ij}} l_{\mathrm{i}} l_{\mathrm{j}}$ and $G_{\mathrm{ij}} = \sum_k g_{\mathrm{ik}} g_{\mathrm{kj}}$, where l_{i} (i = x, y, z) are the direction cosines of the static field for a set of orthogonal axes (x, y, z) fixed in the crystallographic axes (a*, b, c*), respectively. The principal g-values are determined as $g_1 = 2.0118$, $g_2 = 2.0063$, and $g_3 = 2.0025$, and the principal axes are in agreement with the c*-, a*-, and b-axes, respectively, within the experimental error.

Figure 7 shows the temperature dependence of the g-value, linewidth (ΔH_{pp}), and spin susceptibility (χ_{spin}) estimated from the EPR signal. The

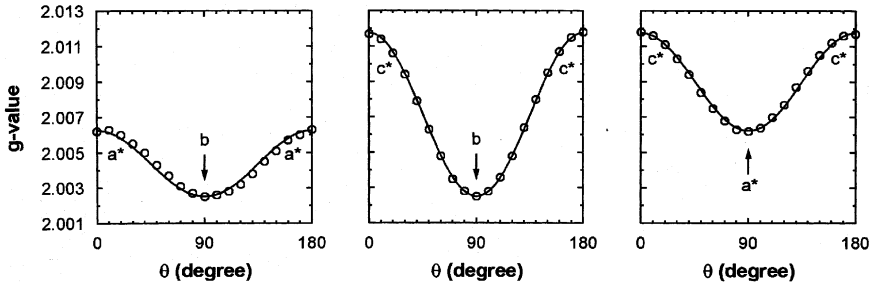

FIGURE 6 The angle dependence of the g-factor for α'-$(EOET)_2AuBr_2$ at RT applying the static magnetic field within (a) a^*b-, (b) bc^*-, and (c) c^*a^*-planes. Solid curves are the least squares fit to the measured data (see text).

Downloaded by [University of Haifa Library] at 10:53 11 August 2012

g-values remain invariant down to *ca*. 20 K, where the values applying the static magnetic field along the a^*- and c^*-axes rapidly decrease, while that along the b-axis shows a slight upturn. The RT χ_{spin} value of *ca* 1.1×10^{-3} emu mol^{-1} is in good agreement with that estimated from the static susceptibility measurement. With decreasing temperature it exhibits a rounded maximum at around 160 K and then continuously drops down to 12 K. The different χ_{spin} behavior from that by SQUID may be caused by the temperature-dependent cavity Q value. A sharp upturn of the EPR intensity was observed at temperatures $9 \leq T \leq 12$ K, followed by a rapid decreasing of χ_{spin} toward zero almost completely within the temperature range of $\Delta T \sim 3$ K. Along with these findings, there is a remarkable broadening of the EPR signal below 12 K, strongly indicating the development of 3D AF fluctuations below that temperature and a long-range AF ordering below 9 K. No additional signal, expected as an antiferromagnetic resonance, was observed under the magnetic field of $0 \leq H_0 \leq 12$ kOe down to 4 K. Such a long-range AF ordering with Néel temperature $T_N \sim 9$ K has not been realized for α'-ET salts, most of which are modeled by low-dimensional AF fluctuations down to low temperatures [12].

In comparison with the spin geometry of α'-$(EOET)_2AuBr_2$ depicted in Figure 5b, α'-ET salts have no relative shift of dimers along the stack with respect to dimers within the neighboring stack, (Figure 8) [12]. In the case of α'-$(ET)_2AuBr_2$, which shows low-dimensional AF fluctuations down to 4 K [12e], the averaged t'/t value is estimated to 0.25, indicating a 2D square lattice layer similar to α'-$(EOET)_2AuBr_2$. The averaged t value of 2.1×10^{-2} eV is rather smaller than that of α'-$(EOET)_2AuBr_2$ (3.0×10^{-2} eV), and would be closely connected with the smaller $|J|/k_B$ value for the QLAF model (39.5 K) than that of α'-$(EOET)_2AuBr_2$ (60–70 K). It is thus probable

Downloaded by [University of Haifa Library] at 10:53 11 August 2012

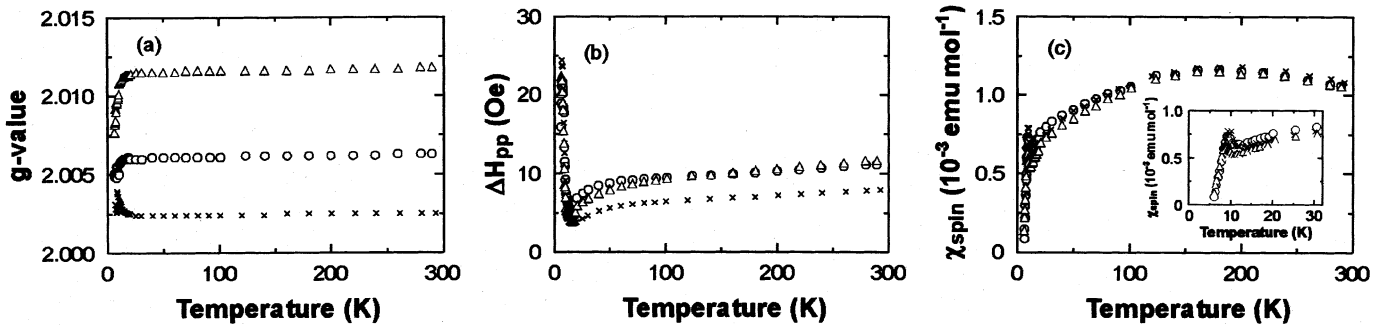

FIGURE 7 Temperature dependence of (a) the g-value, (b) the linewidth, and (c) the spin susceptibility of the EPR signal of α'-$(EOET)_2AuBr_2$ applying the static magnetic field along the a^*- (o), b- (×), and c^*- (Δ) axes.

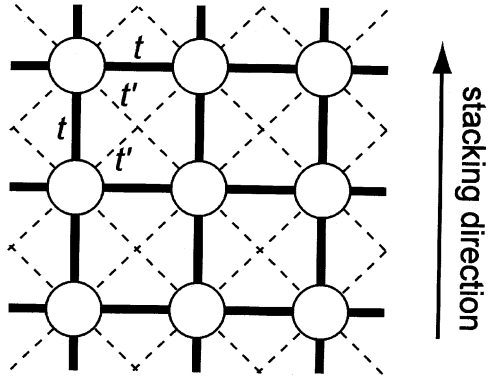

FIGURE 8 Schematic square spin-geometry of α'-ET salts based on a spin-1/2 ET dimer (circle). Solid and dotted lines linking the circles represent the transfer interactions with the absolute value more than 1×10^{-2} eV and less than 1×10^{-2} eV, respectively, for α'-$(ET)_2AuBr_2$.

Downloaded by [University of Haifa Library] at 10:53 11 August 2012

that α'-$(ET)_2AuBr_2$ also exhibits the AF ordering at further low temperatures. This is currently under study.

β''-$(EOET)_2AuBr_2$

The crystallographic data are summarized in Table I. One donor molecule and a half anion molecule are crystallographically independent, and no orientational disorder was observed in the EOET molecules unlike the α'-salt. The EOET molecules form a segregated column along the $(a-b)$-axis and the columns form a 2D layer with short S··S and S··O intermolecular contacts (3.455(4) and 3.506(4) Å for S_{in}··S_{in}, 3.243(8) Å for S_{in}·· Figure 9a) in the ab-plane. The donor packing pattern is analogous to the β''-phase of ET salts, which have both 2D holelike and waved 1D electron-like Fermi surfaces and are metallic down to low temperatures [17]. Figures 9b and c show the relative arrangements between two neighboring EOET molecules. The patterns A and D include short CH··O contacts of 3.65(2) and 3.62(2) Å, and the patterns B and D include short CH··S contacts of 3.79(1)–3.81(1) and 3.93(1) Å, respectively. The sliding pattern along the molecular long axis in B has never been realized in BO salts. However, the short S_{in}··S_{in} contacts of 3.506(4) and 3.455(4) Å were observed in C and E, respectively, in a fashion similar to the BO salts. Although the effectiveness of the CH··S contacts is not certain, the presence of the CH··O contacts together with the S_{in}··S_{in} ones strongly indicate the self-assembling nature of the EOET molecules, resulting in the formation of the 2D electronic

Downloaded by [University of Haifa Library] at 10:53 11 August 2012

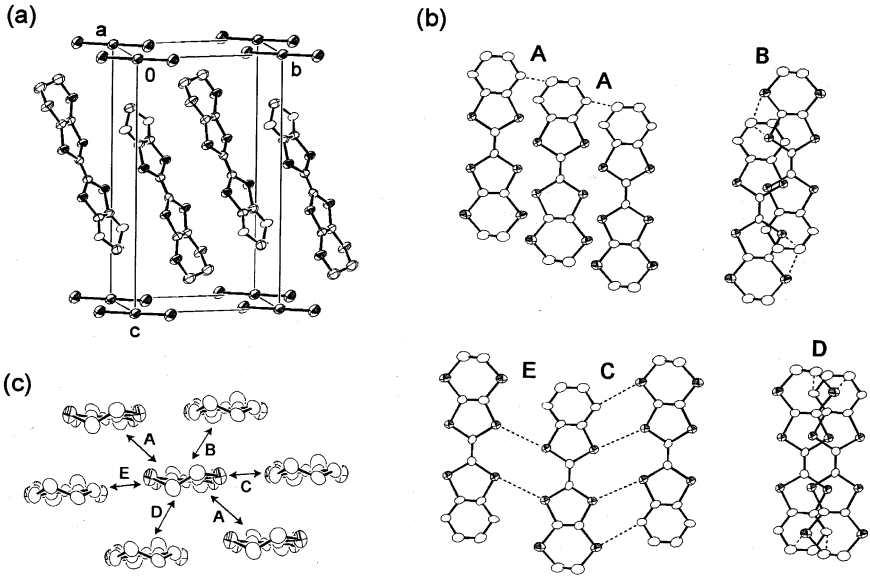

FIGURE 9 (a) Crystal structure, (b) relative arrangements between two neighboring EOET molecules (A–E) where atomic contacts shorter than the sum of the van der Waals radii are indicated by dotted lines, and (c) donor layer viewed along the molecular short axis for β''-(EOET)$_2$AuBr$_2$.

structure. The overlap integral for each pattern is estimated to -4.28, -2.07, -2.28, -0.19, and -2.60×10^{-3} for A–E, respectively. The energy dispersion, density of states, and Fermi surface calculated by the extended Hückel method are depicted in Figure 10.

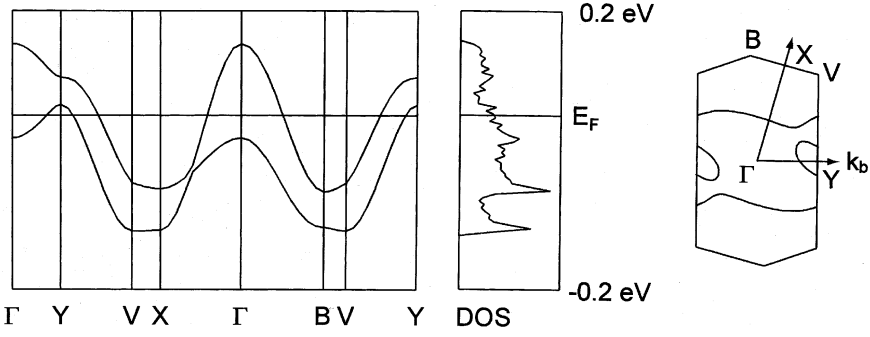

FIGURE 10 Band structure, density of states (DOS), and Fermi surface based on the extended Hückel calculation by the tight binding approximation for β''-(EOET)$_2$AuBr$_2$.

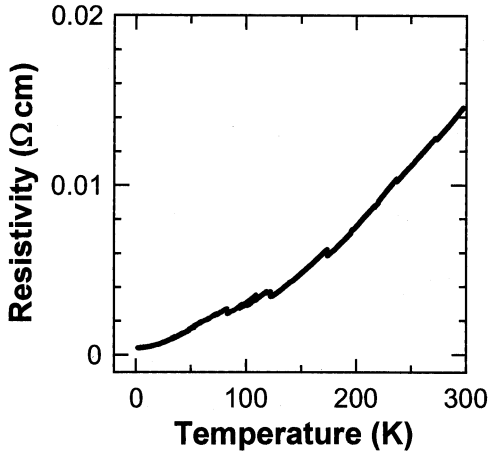

FIGURE 11 Temperature dependence of electric resistivity of β''-$(EOET)_2AuBr_2$.

The calculated Fermi surface is composed of a big ellipsoid centered at Γ-point and then folded to give a 2D hole-pocket centered at Y and wavy 1D electron-like surface along the k_b-direction, that is very similar to those of the metallic salts formed with parent molecules, i.e., β''-$(ET)_2AuBr_2$ [17] and $(BO)_2ClO_4$ [2a], suggesting a metallic nature of β''-$(EOET)_2AuBr_2$.

The UV-Vis-NIR spectrum of the salt displayed in Figure 3 (curve b) is similar to that of the Mott-insulating α'-phase (curve a) with marginal differences; a slight red-shift of the A band and a slight increase of the relative intensity of the band. Nevertheless, unlike the α' salt, the β'' salt shows a simple metallic behavior with $\sigma_{RT} = 6-7\times10\,S\,cm^{-1}$ down to 1.6 K ($\sigma_{1.6K} = 4.2\times10^4\,S\,cm^{-1}$; Figure 11).

SUMMARY

Based on the crystal and electronic structures and physical properties of α'- and β''-type $AuBr_2$ salts of EOET, where EOET is a hybrid donor between ET and BO molecules, we conclude that the α' and β'' salts inherit the features of the ET and BO salts, respectively. The α' salt is a Mott insulator with a spin-1/2 EOET dimer as a unit and follows the quadratic layer antiferromagnetic model above 60 K. Even though the α'-type Mott insulators based on ET usually have not exhibited a long range magnetic order, α'-$(EOET)_2AuBr_2$ shows a long range antiferromagnetic order with $T_N \sim 9$ K. The β''-$(EOET)_2AuBr_2$ shows the nature of self assembling in the crystal and is metallic down to low temperatures similar to many BO compounds.

Downloaded by [University of Haifa Library] at 10:53 11 August 2012

Downloaded by [University of Haifa Library] at 10:53 11 August 2012

REFERENCES

[1] Ishiguro, T., Yamaji, K., & Saito, G. (1998). *Organic Superconductors*, 2nd ed., (Berlin: Springer).

[2] (a) Horiuchi, S., Yamochi, H., Saito, G., Sakaguchi, K., & Kusunoki, M. (1996). *J. Am. Chem. Soc.*, *118*, 8604–8622.
(b) Wudl, F., Yamochi, H., Suzuki, T., Isotaro, H., Fite, C., Kasmai, H., Liou, K., Srdanov, G., Coppens, P., Maly, K., & Frost-Jensen, A. (1990). *J. Am. Chem. Soc.*, *112*, 2461–2462.

[3] (a) Nakamura, T., Yunome, G., Azumi, R., Tanaka, M., Tachibana, H., Matsumoto, M., Horiuchi, S., Yamochi, H., & Saito, G. (1994). *J. Chem. Phys.*, *98*, 1882–1887.
(b) Ogasawara, K., Ishiguro, T., Horiuchi, S., Yamochi, H., & Saito, G. (1996). *Jpn. J. Appl. Phys.*, *35*, L571–L573.
(c) Ohnuki, H., Noda, T., Izumi, M., Imakubo, T., & Kato, R. (1997). *Phys. Rev.*, *B55*, R10225–R10228.
(d) Tracz, A., Jeszka, J. K., Sroczynska, A., Ulanski, J., Plocharski, J., Yamochi, H., Horiuchi, S., & Saito, G. (1997). *Synth. Met.*, *86*, 2173–2174.
(e) Horiuchi, S., Yamochi, H., Saito, G., Jeszka, J. K., Tracz, A., Sroczynska, A., & Ulanski, J. (1997). *Mol. Cryst. Liq. Cryst.*, *296*, 365–382.

[4] Saito, G., Sasaki, H., Aoki, T., Yoshida, Y., Otsuka, A., Yamochi, H., Drozdova, O. O., Yakushi, K., Kitagawa, H., & Mitani, T. (2002). *J. Mater. Chem.*, *12*, 1640–1649.

[5] Terzis, A., Hountas, A., Hilti, B., Mayer, C., Zambounis, J. S., Lagouvardos, D., Kakoussis, V. C., Mousdis, G., & Papavassiliou, G. C. (1995). *Synth. Met.*, *41–43*, 1715–1719.

[6] Konovalikhin, S. V., Shilov, G. V., Zhilyaeva, E. I., Torunova, S. A., & Lyubovskaya, R. N. (2000). *Russ. J. Coord. Chem.*, *26*, 89–96.

[7] Papavassiliou, G. C., Lagouvardos, D., Kakoussis, V. C., Terzis, A., Hountas, A., Hilti, B., Mayer, C., Zambounis, J. S., Pffeiffer, J., Whangbo, M.-H., Ren, J., & Kang, D. B. (1992). *Mater. Res. Soc. Symp. Proc.*, *247*, 535–540.

[8] Ducasse, L., Mousdis, G., Fettouhi, M., Ouahab, L., Amiell, J., & Delhaes, P. (1993). *Synth. Met.*, *55–57*, 1995–2000.

[9] Papavassiliou, G. C., Kakoussis, V. C., Lagouvardos, D. J., & Mousdis, G. A. (1990). *Mol. Cryst. Liq. Cryst.*, *181*, 171–184.

[10] (a) Aoki, T., Saito, G., Yamochi, H., & Maesato, M. (2002). *Mol. Cryst. Liq. Cryst.*, *376*, 201–206.
(b) Yoshida, Y., Aoki, T., Yamochi, H., & Saito, G. *Synth. Met.*, in press.

[11] Ramakumar, R., Tanaka, Y., & Yamaji, K. (1997). *Phys. Rev.*, *B56*, 795–801.

[12] (a) Beno, M. A., Firestone, M. A., Leung, P. C. W., Sowa, L. M., Wang, H. H., & Williams, J. M. (1986). *Solid State Commun.*, *57*, 735–739.
(b) Ugawa, A., Yakushi, K., Kuroda, H., Kawamoto, A., & Tanaka, J. (1988). *Synth. Met.*, *22*, 305–315.
(c) Chasseau, D., Watkin, D., Rosseinsky, M. J., Kurmoo, M., Talham, D. R., & Day, P. (1988). *Synth. Met.*, *24*, 117–125.
(d) Watson, W. H., Kini, A. M., Beno, M. A., Montgomery, L. K., Wang, H. H., Carlson, K. D., Gates, B. D., Tytko, S. F., Derose, J., Carris, C., Rohl, C. A., & Williams, J. M. (1989). *Synth. Met.*, *33*, 1–9.
(e) Obertelli, S. D., Friend, R. H., Talham, D. R., Kurmoo, M., & Day, P. (1989). *J. Phys.: Condens. Matter*, *1*, 5671–5680.
(f) Parker, I. D., Friend, R. H., Kurmoo, M., & Day, P. (1989). *J. Phys.: Condens. Matter*, *1*, 5681–5688.
(g) Ward, B. H., Granroth, C. E., Abboud, K. A., Meisel, M. W., & Talham, D. R. (1998). *Chem. Mater.*, *10*, 1102–1108.
(h) Sekizaki, S., Yamochi, H., & Saito, G. (2001). *Synth. Met.*, *120*, 961–962.

(i) Zaman, Md. B., Toyoda, J., Morita, Y., Nakamura, S., Yamochi, H., Saito, G., Nishimura, K., Yoneyama, N., Enoki, T., & Nakasuji, K. (2001). ***J. Mater. Chem.***, *11*, 2211–2215.
[13] Bondi, A. (1964). ***J. Phys. Chem.***, *86*, 441–445.
[14] Bonner J. C., & Fisher, M. E. (1964). ***Phys. Rev.***, *135*, A640–A658.
[15] Lines, M. E. (1970). ***J. Phys. Chem. Solids.***, *31*, 101–116.
[16] Welp, U., Fleshler, S., Kwok, W. K., Crabtree, G. W., Carlson, K. D., Wang, H. H., Geiser, U., Williams, J. M., & Hitsman, V. M. (1992). ***Phys. Rev. Lett.***, *69*, 840–843.
[17] Mori, T., Sakai, F., Saito, G., & Inokuchi, H. (1986). ***Chem. Lett.***, 1037–1040.

Downloaded by [University of Haifa Library] at 10:53 11 August 2012